Insight into the Coordination and the Binding Sites of Cu^{2+} by the Histidyl-6-Tag using Experimental and Computational Tools

Joanna Watly,[†] Eyal Simonovsky,[‡,§] Robert Wieczorek,[†] Nuno Barbosa,[†] Yifat Miller,*[,‡,§] and Henryk Kozlowski*[,†]

[†]Faculty of Chemistry, University of Wroclaw, 50-383 Wroclaw, Poland

[‡]Department of Chemistry and [§]Ilse Katz Institute for Nanoscale Science and Technology, Ben-Gurion University of the Negev, Beer-Sheva 84105, Israel

Ⓢ *Supporting Information*

ABSTRACT: His-tags are specific sequences containing six to nine subsequent histydyl residues, and they are used for purification of recombinant proteins by use of IMAC chromatography. Such polyhistydyl tags, often used in molecular biology, can be also found in nature. Proteins containing histidine-rich domains play a critical role in many life functions in both prokaryote and eukaryote organisms. Binding mode and the thermodynamic properties of the system depend on the specific metal ion and the histidine sequence. Despite the wide application of the His-tag for purification of proteins, little is known about the properties of metal-binding to such tag domains. This inspired us to undertake detailed studies on the coordination of Cu^{2+} ion to hexa-His-tag. Experiments were performed using the potentiometric, UV−visible, CD, and EPR techniques. In addition, molecular dynamics (MD) simulations and density functional theory (DFT) calculations were applied. The experimental studies have shown that the Cu^{2+} ion binds most likely to two imidazoles and one, two, or three amide nitrogens, depending on the pH. The structures and stabilities of the complexes for the Cu^{2+}-Ac-$(His)_6$-NH_2 system using experimental and computational tools were established. Polymorphic binding states are suggested, with a possibility of the formation of α-helix structure induced by metal ion coordination. Metal ion is bound to various pairs of imidazole moieties derived from the tag with different efficiencies. The coordination sphere around the metal ion is completed by molecules of water. Finally, the Cu^{2+} binding by Ac-$(His)_6$-NH_2 is much more efficient compared to other multihistidine protein domains.
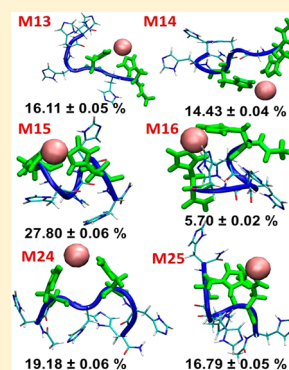
■ INTRODUCTION

More than 2000 histidine-rich proteins (HRPs) have been found in microorganisms including 60% and 82% of archaeal and bacterial species, respectively. The part of those proteins (around 670) consist of His-tag motifs[1] but they have not been well characterized yet.[2] Proteins containing histidine-rich domains play a critical role in metal regulation and homeostasis.[3,4] Also, other functions of histidine-rich proteins in eukaryotes have been reported,[5,6] e.g. antimicrobial activities in the oral cavity (histatins from saliva),[7] heme polymerization (HRP-2 from *Plasmodium falciparum*),[8] or heparin binding (serum glycoprotein HRG found in humans).[9]

One of the basic tools used in the purification of the recombinant proteins are hexa-histidine affinity tags.[10] His-tags are commonly used in molecular biology due to their special metal ion binding properties. His-tags are relatively small species; they do not affect protein folding and thus do not interfere significantly with the biological functionality of the target proteins. Extensive studies have been performed on copper, zinc, and nickel binding to His-containing model peptides. The binding of metal ions are really specific as far as both binding mode and their thermodynamic characteristics are concerned.[11−17] Thus, the binding ability of His-tags seems to be basic for both synthetic and natural protein functioning.

Immobilized metal ion affinity chromatography (IMAC) is the most common method for purifying histidine-tagged proteins.[18] The imidazole rings of histidines play a role as donor groups that have the ability to form coordination bonds with the immobilized transition metal. Nitrilotriacetic acid (NTA) adsorbent is the most commonly used chelator of metal ions in IMAC technique. The NTA resin is used along with the metal ion with coordination number of six, to form a tetradentate chelate.[19] Ni^{2+} or other metal ions immobilized on the surface-bound chelators such as NTA[20] are able to field highly enriched proteins from crude extracts in a one-step purification procedure.[21] Mechanisms of binding of hexa-histidine-tags to Ni^{2+}-NTA surfaces were studied with the surface plasmon resonance (SPR) technique.[22] This study has shown that the hexa-histidine-tag has the best affinity toward metal ions involving two histidines (imidazoles) separated by one or four residues. The length of six residues in the His-tag had been found to be the best effective affinity to metal ions. Therefore, both the elongation and shortening of the His-tag chain decrease the metal ion binding efficiency to the His-tag.

The affinity of a protein to a metal chelate strongly depends on the type of the metal ion involved in the coordination. The

binding of two imidazoles to an immobilized metal ion is rather comprehensible behavior, assuming that bound Ni^{2+} ion involves four other binding sites to coordinate the NTA chelator. Previously, molecular dynamic (MD) calculations also have shown involvement of two imidazoles in the metal ion binding for Ni^{2+}, Cu^{2+}, Zn^{2+}, and Co^{2+} ions.[23]

So far, experimental techniques are limited to give information on the specific binding sites of metal ions with fragments of poly-His. In this study we combine experimental techniques, molecular dynamics (MD) simulations, and density functional theory (DFT) calculations in the aim of giving insight into the coordination and the structural binding sites of Cu^{2+} in the C- and N-protected peptide Ac-$(His)_6$-NH_2.

■ EXPERIMENTAL SECTION

Potentiometric Measurements. Potentiometric measurements were performed at a constant temperature of 25 °C under an argon atmosphere using a Molspin pH-meter, equipped with a semi-combined electrode Mettler Toledo InLab Micro and micrometer syringe with a volume of 0.5 cm³.[24] The measurements were performed in a pH range of 2−11. Before each measurement, the electrode was calibrated by titration with HCl having a concentration of 4×10^{-3} M with a strong base NaOH, (0.1 M).

The pH-metric titrations were performed in a water solution of HCl 0.1 M KCl. The titrant was a carbonate-free, standard solution of NaOH. The ligand concentration was 1×10^{-3} M and the metal-to-ligand molar ratios were 1:1.1. Small aliquots of fresh aqueous solutions were used to add metal ions. Stability constants for the proton−Cu^{2+} complexes were calculated from two titrations measured using a total volume of 1.5−1.7 cm³.

The exact concentrations of the ligand and proton were determined by using the Gran method.[25] The data obtained in potentiometric measurements were analyzed using the Hyperquad and Superquad programs. Protonation constants of the ligands and overall stability constants (log βpqr) of the Cu^{2+} complexes were calculated by using eqs 1 and 2.[26,27]

$$p\text{M} + q\text{H} + r\text{L} = \text{M}_p\text{H}_q\text{L}_r \tag{1}$$

$$\beta_{pqr} = \frac{[\text{M}p\text{H}q\text{L}r]}{[\text{M}]^p[\text{H}]^q[\text{L}]^r} \tag{2}$$

Standard deviations were given by the program itself and refer to random errors only. The speciation and competition diagrams were computed using HySS 2006.[28]

UV−Vis, CD, and EPR studies. Measurements of the absorption UV−vis spectroscopy were performed using a Cary 300 Bio spectrophotometer, and CD spectroscopy of the studied systems was measured using spectropolarimeter Jasco J-715 in quartz cuvette path lengths of 0.1 and 1.0 cm, at 25 °C using a total volume of 2−2.5 cm³. A cell with a 1 cm path length was used for spectra recorded between 300 and 800 nm. Spectra were obtained using Jasco Spectra Analysis Software (version 1.53.04).

UV−vis and CD spectra of the Cu^{2+} complexes were recorded in the same concentration range as used for pH titrations. The ligand concentration was 1×10^{-3} M, and the metal-to-ligand molar ratio was 1:1.1.

The EPR spectra were recorded in liquid nitrogen on a Bruker ELEXSYS E500 CW-EPR spectrometer at X-band frequency (9.5 GHz) and equipped with ER 036TM NMR Teslameter and E41 FC frequency counter. The concentration of Cu^{2+} and peptides were the same as used for pH-potentiometry. Ethylene glycol (30%) was used as a cryoprotectant for EPR measurements. The EPR parameters were obtained by simulation of plots using the Bruker WinEPR SimFonia program.

The UV−vis and CD spectroscopic parameters were calculated from the spectra that were obtained at the pH values corresponding to the maximum concentration of the particular species on the basis of distribution diagrams from the potentiometric studies.

Data were processed using the Origin 7.0.

Mass Spectrometric Measurements. High-resolution mass spectra were obtained using a Bruker Q-FTMS spectrometer (Bruker Daltonik, Bremen, Germany), equipped with an Apollo II electrospray ionization source.

Spectrometer was used in the range of positive values of m/z (mass to charge ratio) from 100 to 1500. The instrumental parameters were as follows: scan range m/z 400−2000, dry gas−nitrogen, temperature 170 °C, ion energy 5 eV, transfer time 120 ps. Capillary voltage was optimized and amounted 4500 V. The small changes of voltage (±500 V) did not significantly affect the optimized spectra. The CuL complex in a 1:1.1 stoichiometry was prepared in 1:1 MeOH−H_2O mixture. The instrument was calibrated by a Tunemix solution. Data were processed by using the Bruker Compass DataAnalysis 4.0 program.

Molecular Dynamics (MD) Simulations Protocol. We constructed six models of the Cu^{2+}-Ac-$(His)_6$-NH_2 complex. As one can see, the $(His)_6$ peptide had been capped in the N-terminal to Ac and to NH_2 in the C-terminal. We considered all the possible varieties that Cu^{2+} can bind to the peptide Ac-$(His)_6$-NH_2. In model M13 the Cu^{2+} binds to His1 and His3, in model M14 the Cu^{2+} binds to His1 and His4, in model M15 the Cu^{2+} binds to His1 and His5, in model M16 the Cu^{2+} binds to His1 and His6, in model M24 the Cu^{2+} binds to His2 and His4, and in model M25 the Cu^{2+} binds to His2 and His5. The six models were first minimized as we have previously performed for amyloids and other peptides.[29−32] MD simulations of the solvated models were performed in the NPT ensemble using NAMD[32] with the CHARMM27 force-field.[34,35] The models were energy minimized and explicitly solvated in a TIP3P water box[36,37] with a minimum distance of 15 Å from each edge of the box. Each water molecule within 2.5 Å of the models was removed. Counter ions were added at random locations to neutralize the models' charge. The Langevin piston method[29,38,39] with a decay period of 100 fs and a damping time of 50 fs was used to maintain a constant pressure of 1 atm. A temperature of 310 K was controlled by a Langevin thermostat with a damping coefficient of 10 ps.[29−33] The short-range van der Waals interactions were calculated using the switching function, with a twin range cutoff of 10.0 and 12.0 Å. Long-range electrostatic interactions were calculated using the particle mesh Ewald method with a cutoff of 12.0 Å.[40,41] The equations of motion were integrated using the leapfrog integrator with a step of 1 fs. The solvated systems were energy minimized for 2000 conjugated gradient steps, where the hydrogen-bonding distance between the β-sheet in each oligomer was fixed in the range 2.2−2.5 Å. The counterions and water molecules were allowed to move. The hydrogen atoms were constrained to the equilibrium bond using the SHAKE algorithm.[42]

The minimized solvated systems were energy minimized for 5000 additional conjugate gradient steps and 20,000 heating steps at 250 K, with all atoms being allowed to move. Then, the system was heated from 250 to 310 K for 300 ps and equilibrated at 310 K for 300 ps. All simulations were run for 30 ns at 310 K.

Generalized Born Method with Molecular Volume (GBMV). The relative conformational energies can be compared only for models that have the same sequence and number of peptides; thus, the relative conformational energies had been computed for all six models. To obtain the relative conformational energies of the six models, the models' trajectories of the last 5 ns were first extracted from the explicit MD simulations excluding the water molecules—a total of 500 conformations for each oligomer. The solvation energies of all conformations were calculated using the GMBV.[43,44] In the GBMV calculations, the dielectric constant of water was set to 80. The hydrophobic solvent-accessible surface area (SASA) term factor was set to 0.00592 kcal/(mol Å). Each conformation was minimized using 1000 cycles, and the conformational energy was evaluated by grid-based GBMV.

A total of 3000 conformations (500 for each model) were used to construct the energy landscape of the six models and to evaluate the conformer probabilities by using Monte Carlo (MC) simulations. In the first step, one conformation of conformer i and one conformation of conformer j were randomly selected. Then, the Boltzmann factor was computed as $e^{-(E_j-E_i)/kT}$, where E_i and E_j are the conformational

Table 1. Potentiometric and Spectroscopic Data for Proton and Cu^{2+}- Ac-(His)$_6$-NH$_2$ Complexes in Aqueous Solutions; [Cu^{2+}] 0.0009 M; Cu^{2+} to ligand ratio of 1:1.1

species	log β	pKa	proposed donors	UV−vis λ/nm	UV−vis ε/M^{-1} cm^{-1}	CD λ/nm	CD $\Delta\varepsilon$/M^{-1} cm^{-1}	EPR $A_{\parallel}$ (G)	EPR $g_{\parallel}$
HL	7.53(3)	7.53							
H$_2$L	14.13(2)	6.6							
H$_3$L	20.65(3)	6.52							
H$_4$L	26.38(3)	5.73							
H$_5$L	31.98(3)	5.6							
H$_6$L	36.78(3)	4.8							
CuH$_4$L	31.67(7)		2N$_{im}$	655	29				
				307	56				
CuH$_3$L	27.44(5)	4.22	2N$_{im}$	602	38			156	2.29
				319	111				
CuH$_2$L	23.08(3)	4.36	2N$_{im}$	571	44	647	−0.21		
				319	124	531	0.97		
						317	−0.59		
CuHL	17.89(3)	5.19	2N$_{im}$, N$^-$	568	47	643	−0.23	184	2.23
				319	128	531	1.03		
						318	−0.65		
CuL	11.53(5)	6.36	2N$_{im}$, N$^-$	565	52	649	−0.09	188	2.24
				308	165	520	0.84		
						330	−0.73		
CuH$_{-2}$L	−4.04(6)		2N$_{im}$, 2N$^-$	544	70	633	0.36	202	2.20
						546	−0.29		
						484	0.31		
						336	−1.42		
						250	5.67		
CuH$_{-3}$L	−14.35(8)	10.31	N$_{im}$, 3N$^-$	533	74	663	1.1	189	2.19
						516	−1.56		
						301	−0.59		
						258	7.38		

energies evaluated using the GBMV calculations for conformations i and j, respectively; k is the Boltzmann constant, and T is the absolute temperature (298 K used here). If the value of the Boltzmann factor was larger than the random number, then the move from conformation i to conformation j was allowed. After 1 million steps, the conformations "visited" for each conformer were counted. Finally, the relative probability of model n were evaluate as $P_n = N_n/N_{total}$, where P_n is the population of model n, N_n is the total number of conformations visited for model n, and N_{total} is the total steps. The advantages of using MC simulations to estimate conformer probability lie in their good numerical stability and the control that they allow of transition probabilities among several conformers.

Using all six models and 3000 conformations (500 for each model) generated from the MD simulations, we estimated the overall stability and populations for each conformer based on the MD simulations, with the energy landscape being computed with GBMV for these six models. The group these six models is likely to present may be only a very small percentage of the ensemble. Nevertheless, the carefully selected models cover the most likely structures.

Density Functional Theory (DFT) Calculations. Quantum calculations are valuable tools to predict the structure and the stability of the Cu^{2+}-Ac-(His)$_6$-NH$_2$ complexes.[45−47] Molecular orbital studies on Cu^{2+} cation 1:1 complex with capped Ac-(His)$_6$-NH$_2$ peptide have been done on the DFT level of theory. All calculation were performed with Gaussian 09 suite of programs[48] using the M05-2X[49] hybrid functional and the 6-311G(d,p) basis set. The starting structure for DFT calculations was generated on the basis of the amino acid sequence of Ac-(His)$_6$-NH$_2$ capped peptide after 75 ns simulation at 300 K, without cutoffs using BIO+ implementation of CHARMM force field (structures M23 and M45)[50] as well as GBMV for structures M13 and M24.

■ RESULTS AND DISCUSSION

The Ratio of Cu^{2+}-Ac-(His)$_6$-NH$_2$ Complexes. The terminal amino groups of peptides are the most common anchors for metal binding. Therefore, Cu^{2+} which is complexed with free C- and N- termini peptides or with protected peptides may give significantly different results. In this work we studied the terminally protected hexa-histidine peptide.

To investigate the structural and thermodynamic properties of Cu^{2+}-Ac-(His)$_6$-NH$_2$ complexes we applied mass spectrometry (MS), potentiometric titrations, circular dichroism (CD) and electron paramagnetic resonance (EPR) spectroscopy depending on pH. The MS measurements revealed the stoichiometry of the metal complexes, indicating that only equimolar species are present in the solution (Figure S1 in the Supporting Information [SI]). Ac-(His)$_6$-NH$_2$ forms only equimolar complexes with Cu^{2+} at m/z 963.3. To confirm the signals in the MS a comparison between the experimental signals and the simulations signal showed an excellent agreement.

Determining protonation of Ac-(His)$_6$-NH$_2$ hexa-His-tag the six protonation constants were established which can be assigned to six imidazoles, H$_x$L, where x = 1−6 (as seen in Table 1: pKa's of H$_x$L are 7.53; 6.6; 6.52; 5.73; 5.6; 4.8). The potentiometric data values for the pKa are in good agreement with those found in the literature for similar systems.[12,51−53]

The titration curves for Ac-(His)$_6$-NH$_2$ and Cu^{2+}-Ac-(His)$_6$-NH$_2$ solutions are seen in Figures S2 and S3 (in the SI). The titration curves for Cu^{2+}-Ac-(His)$_6$-NH$_2$ were fitted best by assuming the formation of seven species starting from CuH$_4$L

at pH 3, by the CuH_3L, CuH_2L, $CuHL$, CuL, $CuH_{-2}L$ to $CuH_{-3}L$ at pH above 10.

To investigate the coordination mode of Cu^{2+} with the Ac-$(His)_6$-NH_2 we applied potentiometric titration and spectroscopic techniques, including UV−vis (Figure 1), CD (Figure 2), and EPR (Figure S4 in the SI).
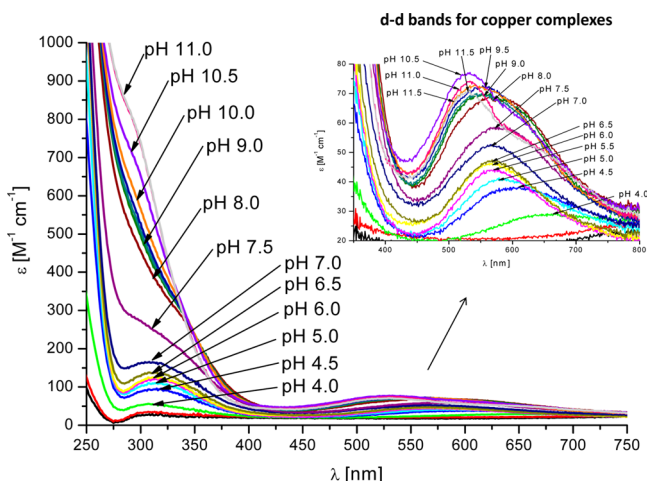
Figure 1. UV−vis spectra for Cu^{2+}-Ac-$(His)_6$-NH_2 complex in aqueous solution. $[Cu^{2+}]$ 0.0009M. Cu^{2+}-to-ligand ratio of 1:1.1.
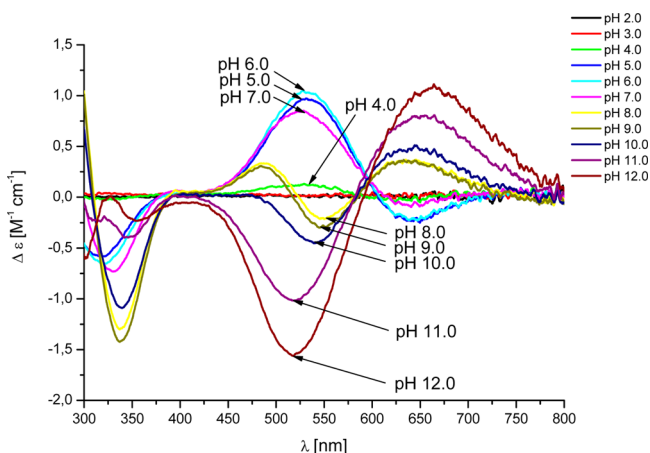
Figure 2. CD spectra for Cu^{2+}-Ac-$(His)_6$-NH_2 complex in aqueous solution. $[Cu^{2+}]$ 0.0009M. Cu^{2+}-to-ligand ratio of 1:1.1. Cuvette path length 1 cm.

The corresponding $\log K^*$ value, which refers to the reaction $Cu^{2+} + H_4L \leftrightarrow CuH_4L$ {$\log K^* = \log \beta(CuH_4L) - \log \beta(H_4L)$} (5.28) in this system suggests the involvement of two imidazole rings in copper coordination.[54,55] The CuH_3L (maximum concentration at 4.5 pH) and CuH_2L (maximum concentration at 5.5 pH) species could arise from the deprotonation of the histidyl imidazoles not taking part in the metal ion complexation. Thus, CuH_3L and CuH_2L are the species with coordination of two imidazoles.

The first complex, confirmed by the spectroscopic data, is $CuHL$. The $CuHL$ species is probably a two-imidazole and one-amide complex. The involvement of amide nitrogens is confirmed by characteristic charge transfer transitions detected in the CD spectra: $N^- \rightarrow Cu^{2+}$ at 319 nm and intense d−d band appearing at pH 5. The d−d band at 568 nm with $\varepsilon = 47.5$ (M^{-1} cm^{-1}) in the UV−vis spectra and EPR parameters

($A_{\parallel}$ 184, $g_{\parallel}$ = 2.23) strongly supported such coordination of both amide and imidazole nitrogens.[56,57]

For CuL species and the lack of the changes in the CD and EPR spectra (Table 1) indicate the deprotonation of the last imidazole nitrogen, which is not bound to Cu^{2+} ion. The pKa value is similar to that of the histidyl imidazole residue in the free ligand (pKa = 6.36).

Two successive deprotonation steps lead to the $CuH_{-2}L$ species. In this case, it is likely that a second deprotonated amide is involved in coordination to copper ion, thus resulting in a $\{2N_{im}, 2N^-\}$ donor set. The absorption band at 553 nm in the UV−vis spectra and EPR parameters ($A_{\parallel}$ = 202 G and $g_{\parallel}$ = 2.20) obtained for $CuH_{-2}L$ (at pH 9) are typically for 4N complexes as well. The 4N coordination is supported by the set of nine hyperfine lines with A_N = 14.2 G. The blue-shift from 553 to 530 nm could derive from the involvement of the consecutive amide nitrogen.[58,59]

A significant change in the CD spectra (inversion of the metal-centered d−d bands) can be observed above pH 11 (Figure 1), and this change suggests also the involvement of a third amide-nitrogen in the coordination of Cu^{2+} resulting in the $\{N_{im}, 3N^-\}$ binding mode.

The involvement of imidazole nitrogens for $CuH_{-2}L$ and $CuH_{-3}L$ species is confirmed by characteristic charge transfer transitions detected in the CD spectra $N_{im} \rightarrow Cu^{2+}$ at 330 nm.[60] Finally, the EPR spectra confirm the assumed all modes of coordination (Figure S4). Binding of the successive nitrogen donors results in the increase of $A_{\parallel}$ and decrease of $g_{\parallel}$ parameters.

Table 1 summarizes the experimental data and the proposed binding coordination. The results indicate good agreement with those found in the literature for similar systems.[56−60]

Structures and Binding Sites of Cu^{2+} in Ac-$(His)_6$-NH_2. One of the most interesting and challenging topics in His-tags is to give an insight into the binding sites of Cu^{2+} and to study the effect of the Cu^{2+} on the structure of the His-tag. Aiming to give an insight into the structure of the Cu^{2+}-Ac-$(His)_6$-NH_2 complex we applied DFT calculations and MD simulations to investigate the structures of Cu^{2+}-Ac-$(His)_6$-NH_2 complexes. The experimental measurements suggest that the Cu^{2+} binds two imidazole groups and/or amide nitrogens. We therefore constructed models and examined their structures using computational tools. Previously, it has been suggested by SPR techniques that the hexa-His-tag is involved in the binding to Cu^{2+} of two imidazole groups which are separated by one or four residues.[22] In this study, we constructed models that Cu^{2+} interacts with two imidazole groups that are separated by up to four residues, considering all possibilities in Ac-$(His)_6$-NH_2: a total of six possible constructed models. We then ran MD simulations to investigate their structures. Figure 3 demonstrates the six simulated models: M13, M14, M15, M16, M24, and M25. Two of these models, M13 and M24, were also computed using DFT calculations (Figure 4). Finally, we also applied DFT calculations for the constructed models M23 and M45 that present two following histidines that bind Cu^{2+} in an aim to examine their structure and their stability (Figure 4).

One can see that in the result of MD simulations among the six models only model M15 showed a well-defined secondary structure of α-helix, as seen from the Ramachandran plot (Figure S5 in the SI), while the other models showed random coil structure. Interestingly, model M15 is energetically more stable (Table S1) and more preferred (Figure 3) than the other models. Model M15 is ~2 times more populated than models
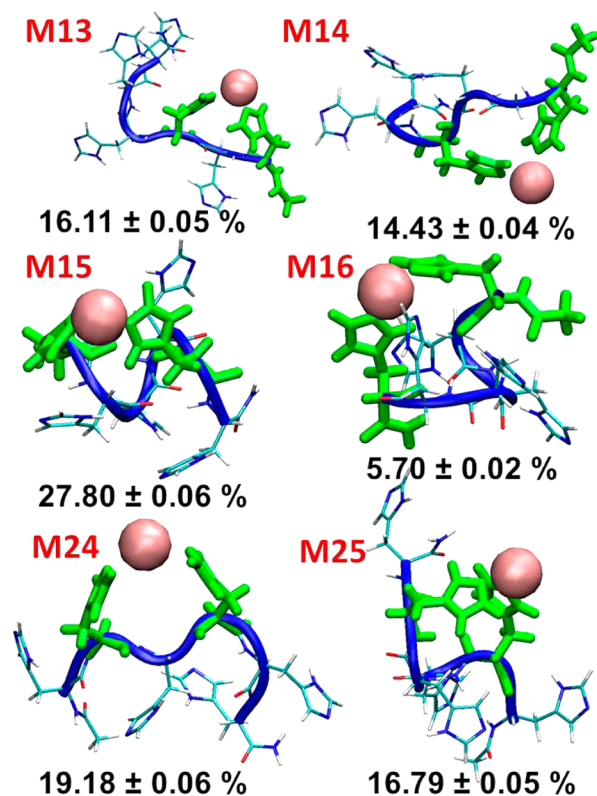
Figure 3. Six constructed models of Cu^{2+}-Ac-(His)$_6$-NH$_2$ complex after MD simulations of 30 ns. In model M13 the Cu^{2+} binds to His1 and His3, in model M14 the Cu^{2+} binds to His1 and His4, in model M15 the Cu^{2+} binds to His1 and His5, in model M16 the Cu^{2+} binds to His1 and His6, in model M24 the Cu^{2+} binds to His2 and His4, and in model M25 the Cu^{2+} binds to His2 and His5. Histidines colored in green bind to Cu^{2+}. The populations and the standard deviations are obtained using the GBMV method[43,44] and Monte Carlo simulations.
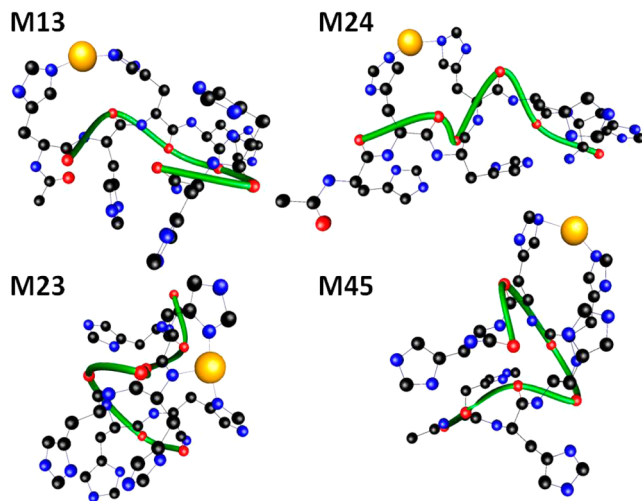
Figure 4. Cu^{2+}-Ac-(His)$_6$-NH$_2$ complex structures calculated at the DFT level of theory. Green tubes follow the backbone.

M13, M14, M24, and M25 and almost 5 times more populated than model M16. Yet, one cannot neglect that models M13, M14, M24, and M25 have similar energies and similar populations; therefore, we suggest an ensemble of polymorphic states for Cu^{2+}-Ac-(His)$_6$-NH$_2$ complex, with a preference for the formation of α-helix structure. Model M15 fluctuates less

during the simulations and therefore is energetically and structurally more stable.

We further investigated the constructed models M13 and M24 using the DFT calculations. The minimized structures are seen in Figure 4. Interestingly, the minimized structure M13 that was obtained by DFT calculations is structurally similar to the M13 that had been obtained from MD simulations. Furthermore, this model M13 illustrates also two imidazole groups that bind Cu^{2+} to form only one C=O···H−N hydrogen bond that forms an α-helical-like structure.

Peptides have versatile ability to build an extended network of intramolecular hydrogen bonds.[61] On one hand we observe typical backbone−backbone interaction to which one can assign regular structure formation, on the other hand histidine-rich peptides are able to gain such stabilization since the imidazole ring can play the roles of proton donor and proton acceptor.

According to the DFT calculations model M24, which also demonstrates two imidazole groups binding Cu^{2+}, did not show α-helical structure. This result is in agreement with the model M24, which had been investigated by MD simulations. The DFT calculations suggest that model M24 is stabilized by five hydrogen-bond (HB) interactions, one between two imidazoles and four between imidazoles and two backbone imidazole···H−N and two imidazole···O=C. One can find synthetic HB networks for DFT investigated complexes in the SI (Figure S6).

The experimental measurements suggested that also the amide bond can bind the Cu^{2+}. All the possible models that demonstrated Cu^{2+} binds to histidines that are separated by 1−4 residues did not show that Cu^{2+} also binds to the amide bond. We therefore constructed two models, M23 and M45, to examine the following two histidines that bind Cu^{2+} using DFT calculations. Interestingly, while M23 showed Cu^{2+} binds to two imidazole groups and an amide bond, model M45 showed Cu^{2+} binds only to two imidazole groups. Model M23 illustrates additional stabilizations of internal HB interactions: five interactions between the imidazole ring and carbonyl groups, one between C=O···H−N fragments of backbone that follows an α-helical pattern of hydrogen bonds (13 atoms create C=O···H−N ring) and one HB interaction between imidazoles. We therefore expect that this model is in lower pH as deprotonated amide nitrogens can be exposed to bind metal ions. Furthermore, model M23, that illustrates a total of three ligands that bind Cu^{2+} (two imidazole groups, and an amide bond), is more stable than model M45 that has a total of only two ligands (two imidazole groups). Model M45 also has complex network of internal hydrogen bonds that consists of five stabilizing interactions: two between a carbonyl group and an imidazole ring, one α-helical C=O···H−N, and one between two imidazoles. M13 complex involves the most fragments of backbone into HB; we have found four N−H···O=C (backbone···backbone) HB organized in a cooperative chain of five formamide-like fragments of backbone and one interaction between imidazole and carbonyl. We gathered the type and number of hydrogen bonds found in DFT-investigated structures in Table S2 in the SI. Therefore, both models M23 and M45 have α-helical structural motifs, due to the hydrogen bonds that are involved with side chain−side chain interactions. Previously, we have shown that short peptides are unable to form stable α-helices;[62] however, the presence of the α-helical motifs close to the metal−peptide binding area suggest that the Cu^{2+} presence can simplify the folding of short peptides. Due to the limitation of the DFT

calculations, we were not able to compute and examine a large number of models of complexes, which may probably be able to show structures that will not form α-helical motifs, as we have shown in the MD simulations for other models.

The DFT calculations showed that Ac-(His)$_6$-NH$_2$ is an effective ligand for Cu^{2+} and can form several different structures of complexes. The most favorable Cu^{2+} binding sites in Ac-(His)$_6$-NH$_2$ are two imidazole groups; however, it is known that Cu^{2+} has the ability to form also other coordination possibilities, such as 3 and 4. We found one model that binds two imidazole groups and an amide bond, but we were not able to find models that bind three or more imidazoles due to the relatively short peptide. In short peptides, the distortion energy of the backbone prevents a suitable topology of imidazole rings to form coordination of more than three imidazole groups. Interestingly, along the MD simulation of two models (M14 and M16) we noticed a third histidine (His5) in the Cu^{2+}-Ac-(His)$_6$-NH$_2$ complex that also binds to the Cu^{2+}. It should be noted that the event of three histidines binding to Cu^{2+} appears around 11% from the snapshots for M14 and 16% of the snapshots in M16, and only around 4.5% of all six simulated models. Therefore, since this event is rare, it is probably difficult to be determined by experiment. However, we expect that models with three or more imidazole groups that bind Cu^{2+} may be possible in histidine-rich long peptides and proteins. The amide bond in metal binding may increase the possibility to form backbone−Cu^{2+} interaction as seen in model M23 (Figure 4). The Cu^{2+} in the Ac-(His)$_6$-NH$_2$ peptide can access the amide bond without breaking the imidazole−Cu^{2+} interactions and without forming distortion of the backbone.

Coordination of Cu^{2+} with Solvating Water Molecules. The experimental procedure is performed in water solution; thus, it is of interest to understand how many water molecules can interact with Cu^{2+}, in addition to the two imidazole groups, as seen in models that are illustrated in Figure 3. It is known that Cu^{2+} has a coordination number of 4, 5, or 6 in biological systems.[63] In the models that are seen in Figure 3, the Cu^{2+} binds two histidines. Therefore, we suggest that it also coordinates to water molecules to form coordination numbers of 4, 5, or 6. To this aim, we followed the number of water molecules that coordinate with the Cu^{2+} along the MD simulations, considering three different cutoff distances between Cu^{2+} and the O atom of the water molecule for each model. To choose the cutoff distances between Cu^{2+} and O atom of the water molecule we used the experimental data on the geometry and constitution metal coordination groups in metalloproteins.[64] The information is derived from protein crystal structures in the Protein Data Bank (PDB), which have been determined by diffraction methods. It has been proposed by CSD that the distance between Cu^{2+} and the O atom of water is 2.13 Å. However, this distance that had been observed by CSD showed a disagreement with the PDB. This disagreement may be because the interactions between Cu^{2+} and the O atom of water are less covalent or more electrostatic or because variations in the coordination number are due to Jahn−Teller distortion.[65] Table S3 in the SI summarizes the distance ranges of Cu^{2+} and the O atom of water for various coordination numbers. The sum of ionic radii of Cu^{2+} and O$_2$ is 1.95 Å; thus, a distance below this value is meaningless. Therefore, we chose three distances: 2.13 Å, 2.17, and 2.5 Å. Figure 5 and Figures S7−S11 (in the SI) show the distribution of the number of water molecules that coordinate with Cu^{2+} at these three cutoff distances. One can see similar results for all
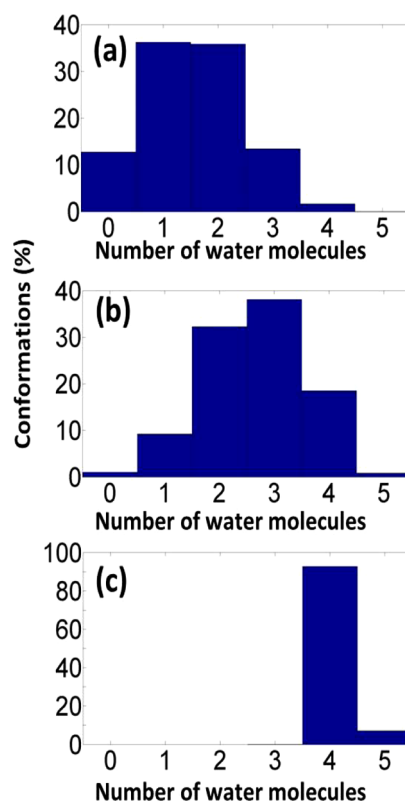
Figure 5. Distribution of the number of water molecules of Cu^{2+}-Ac-(His)$_6$-NH$_2$ complex that coordinate with the Cu^{2+} ions in model M13 according to the cutoff distance of Cu^{2+}−oxygen atom of H$_2$O water molecules: (a) 2.13 Å (b) 2.17 Å and (c) 2.5 Å.

six models: for the cutoff distance of 2.13 Å, only one or two water molecules coordinate with Cu^{2+}; for 2.17 Å, two or three water molecules; and for 2.5 Å, four water molecules coordinate with Cu^{2+}. In summary, the coordination number in the solvate Cu^{2+}-(His)$_6$ complex may be 3, 4, 5, or 6: two histidines and 1, 2, 3, or 4 water molecules.

Ac-(His)$_6$-NH$_2$ Peptide Binds Cu^{2+} More Efficiently than Other Histidine-Rich Protein Domains. In this study we investigated the binding of Cu^{2+} with Ac-(His)$_6$-NH$_2$ peptide. It is of interest also to compare the results of this peptide with the binding of Cu^{2+} with other polyhystidyl protein domains. The histidine-rich domain of Hpn (wild-type Ac-THHHHYHGG-NH$_2$ fragment of Hpn) consists of 5 His residues and one Tyr residue between His 4 and His5. Figure 6 shows the comparison of the binding ability between Ac-(His)$_6$-NH$_2$ peptide and Ac-THHHHYHGG-NH$_2$ peptide. The competition plot shows that Ac-(His)$_6$-NH$_2$ is slightly more efficient in Cu^{2+} binding than Ac-THHHHYHGG-NH$_2$. Mutations of Tyr to Ala, i.e. T1A (Ac-AHHHHYHGG-NH$_2$) decreases the ability of this mutant to bind the Cu^{2+} (Figure 7), suggesting that the Tyr residue is not involved directly in binding Cu^{2+}, but affects the complex stability.[12]

An interesting comparison had been also made with multihistydyl domains which are separated by other residues such as in a sequence that appears in the zebra fish prion protein: Ac-PVHTGHMGHIGHTGHTGH-NH$_2$. In the latter sequence the imidazole groups are well separated, and therefore, it is expected that their binding to Cu^{2+} would be sterically easier. However, as it is shown in Figure 8, Ac-(His)$_6$-
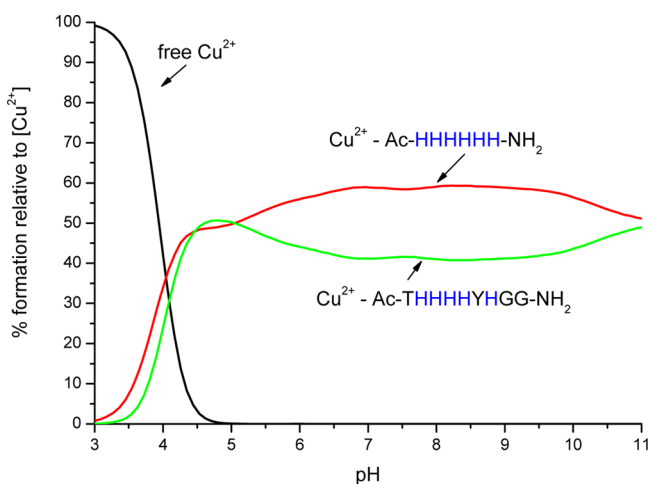
Figure 6. Competition plot of Cu^{2+}-Ac-(His)$_6$-NH$_2$ and Cu^{2+}-Ac-THHHHYHGG-NH$_2$ complexes in aqueous solutions. [Cu^{2+}] 0.0009 M. Cu^{2+}-to-ligand ratio of 1:1.1.
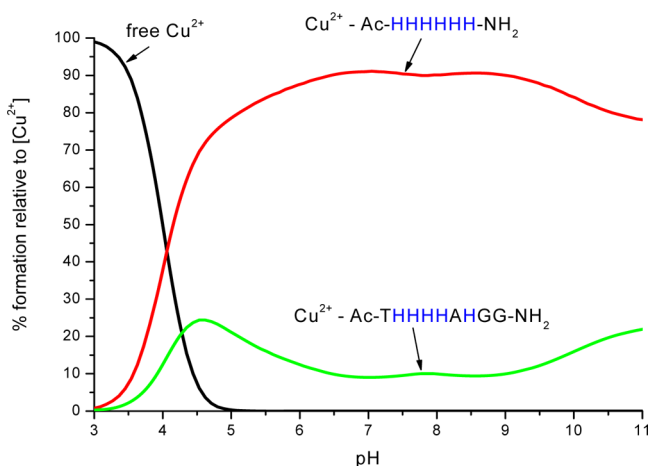
Figure 7. Competition plot of Cu^{2+}-Ac-(His)$_6$-NH$_2$ and Cu^{2+}-Ac-THHHHAHGG-NH$_2$ complexes in aqueous solutions. [Cu^{2+}] 0.0009 M. Cu^{2+}-to-ligand ratio of 1:1.1.

Figure 8. Competition plot of Cu^{2+}-Ac-(His)$_6$-NH$_2$ and Cu^{2+}-Ac-PVHTGHMGHIGHTGHTGH-NH$_2$ complexes in aqueous solutions. [Cu^{2+}] 0.0009 M. Cu^{2+}-to-ligand ratio of 1:1.1.

NH$_2$ peptide is distinctly more effective in binding Cu^{2+} than this peptide.[58]

The exceptional stability of Cu^{2+} species with hexa-histidine-tags could derive from two origins. Our results show that all investigated complexes have strong interactions between the metal cation and two imidazole rings. This is a unique property of hexa-His_ tags because two histidines can be accessed by metal despite the restricted flexibility of a short backbone only due to the imidazole-rich area of the tag. An important part of high stability shall also be assigned to the very rich landscape of hydrogen bonds. We have found six to seven intramolecular hydrogen bonds (depending on the complex structure) involving all types of possible intramolecular interactions in peptides: backbone−backbone, backbone−side chain and side chain−side chain interaction.

CONCLUSIONS

The polyhistidine-tag motif in proteins consists of at least six histidine residues and is located mainly at the C- or the N-terminus of proteins. The most common polyhistidine-tags are formed of six histidine residues. Histidine-tags are widely used because they are small and rarely interfere with the function,

activity, or structure of target proteins. Immobilized metal ion affinity chromatography (IMAC) is the most common method for purifying histidine-tagged proteins. In this study we investigated the binding sites of Cu^{2+} in the Ac-(His)$_6$-NH$_2$. It is interesting that the number of bound imidazoles to one Cu^{2+} ion (two histydyl residues) is similar to what had been previously found by IMAC where the metal ion is immobilized with polydentate chelator.[66,67] Furthermore, the involvement of this hexa-histidine-tag's bond is also likely to be around pH 5.

The MD simulations and DFT calculations have shown that Cu^{2+}-(His)$_6$-NH$_2$ demonstrates polymorphic states with different sets of two bound imidazoles with the first and fifth imidazole bound to metal ion, M15, being the most stable structure. This could suggest that His-tags in proteins may serve as the dynamic site able to move metal ions along the tag sequence. The metal ion binding to imidazoles induces the formation of the α-helical structures for some binding modes, e.g. in M15. This could be the most important finding in this work. Finally, our MD simulations propose that the solvated water molecules complete the coordination sphere around the metal ion.

The effective binding is realized by two imidazoles and two amide nitrogens around pH 9, while at very high pH (around 11) the peptide binding becomes very classical, involving imidazole nitrogen and three amide nitrogens. However, this binding mode is not of biological relevance.

Finally, it is of interest to examine the efficiency of the binding ability to Cu^{2+} of various hexa-histidine-tags motifs in different proteins. Our results showed that the binding ability to Cu^{2+} of the hexa-His-tags is more efficient than in other his-tag motifs in various proteins. The other poly-His sequences that had been examined in this study are characterized by His residues that are well separated and, thus, sterically less available to bind metal ions.

ASSOCIATED CONTENT

S Supporting Information

This material is available free of charge via the Internet at http://pubs.acs.org.

■ AUTHOR INFORMATION

Corresponding Authors

*E-mail: henryk.kozlowski@chem.uni.wroc.pl. Tel: (+48) (71) 375 72 51. Fax: (+48) (71) 375 72 51 (H.K.).

*E-mail: ymiller@bgu.ac.il. Tel: 972-86428705. Fax: 972-86428709 (Y.M.).

Notes

The authors declare no competing financial interest.

■ REFERENCES

(1) Cheng, T.; Xia, W.; Wang, P.; Huang, F.; Wang, J.; Sun, H. *Metallomics* **2013**, *5*, 1423−1429.

(2) Rowinska-Zyrek, M.; Witkowska, D.; Potocki, S.; Remelli, M.; Kozlowski, H. *New J. Chem.* **2013**, *37*, 58−70.

(3) Martino, L.; He, Y.; Hands-Taylor, K. L. D.; Valentine, E. R.; Kelly, G.; Giancola, C.; Conte, M. R. *FEBS J.* **2009**, *276*, 4529−4544.

(4) Witkowska, D.; Rowinska-Zyrek, M.; Valensin, G.; Kozlowski, H. *Coord. Chem. Rev.* **2012**, *256*, 133−148.

(5) Schmitt-Ulms, G.; Ehsani, S.; Watts, J. C.; Westaway, D.; Wille, H. *PLoS One* **2009**, *4*, e7208.

(6) Stanczak, P.; Valensin, D.; Porciatti, E.; Jankowska, E.; Grzonka, Z.; Molteni, E.; Gaggelli, E.; Valensin, G.; H. Kozlowski, H. *Biochemistry* **2006**, *45*, 12227−12239.

(7) Oudhoff, M. J.; Bolscher, J. G.; Nazmi, K.; Kalay, H.; van't Hof, W.; Amerongen, A.; Veerman, E. C. *FASEB J.* **2008**, *22*, 3805−3812.

(8) Trampuz, A.; Jereb, M.; Muzlovic, I.; Prabhu, R. *Crit. Care* **2003**, *7*, 315−323.

(9) Burch, M. K.; Blackburn, M. N.; Morgan, W. T. *Biochemistry* **1987**, *26*, 7477−7482.

(10) Waugh, D. S. *Trends Biotechnol.* **2005**, *23*, 316−320.

(11) Jancso, A.; Kolozsi, A.; Gyurcsik, B.; Nagy, N. V. T.; Gajda, T. *J. Inorg. Biochem.* **2009**, *103*, 1634−1643.

(12) Witkowska, D.; Politano, R.; Rowinska-Zyrek, M.; Guerrini, R.; Remelli, M.; Kozlowski, H. *Chem.—Eur. J.* **2012**, *18*, 11088−11099.

(13) Kozlowski, H.; Potocki, S.; Remelli, M.; Rowinska-Zyrek, M.; Valensin, D. *Coord. Chem. Rev.* **2013**, *257*, 2625−2638.

(14) Kozlowski, H.; Kowalik-Jankowska, T.; Jezowska-Bojczuk, M. *Coord. Chem. Rev.* **2005**, *249*, 2323−2334.

(15) Murariu, M.; Dragan, E. S.; Drochioiu, G. *Biopolymers* **2010**, *93*, 497−508.

(16) Zoroddu, M. A.; Medici, S.; Peana, M. *J. Inorg. Biochem.* **2009**, *103*, 1214−1220.

(17) Migliorini, C.; Witkowska, D.; Valensin, D.; Kamysz, W.; Kozlowski, H. *Dalton Trans.* **2010**, *39*, 8663−8670.

(18) Gaberc-Porekar, V.; Menartr, V. *J. Biochem. Biophys. Methods* **2001**, *49*, 335−360.

(19) Terpe, K. *Appl. Microbiol. Biotechnol.* **2003**, *60*, 523−533.

(20) Hochuli, E.; Dobeli, H.; Schacher, A. *J. Chromatogr.* **1987**, *411*, 177−184.

(21) Lichty, J. J.; Malecki, J. L.; Agnew, H. D.; Michelson-Horowitz, D. J. *Protein Expression Purif.* **2005**, *41*, 98−105.

(22) Knecht, S.; Ricklin, D.; Eberle, A. N.; Ernst, B. *J. Mol. Recognit.* **2009**, *22*, 270−279.

(23) Chen, C.-W.; Liu, H.-L.; Lin, J.-C.; Ho, Y. *J. Chin. Chem. Soc.* **2005**, *52*, 1281−1290.

(24) Irving, H.; Miles, M.; Pettit, L. *Anal. Chim. Acta* **1967**, *38*, 475−488.

(25) Gran, G. *Acta Chem. Scand.* **1950**, *4*, 559−577.

(26) Gans, P.; Sabatini, A.; Vacca, A. *J. Chem. Soc., Dalton Trans.* **1985**, 1195−1199.

(27) Gans, P.; Sabatini, A.; Vacca, A. *Talanta* **1996**, *43*, 1739−1753.

(28) Alderighi, L.; Gans, P.; Ienco, A.; Peters, D.; Sabatini, A.; Vacca, A. *Coord. Chem. Rev.* **1999**, *184*, 311−318.

(29) Miller, Y.; Ma, B.; Nussinov, R. *Proc. Natl. Acad. Sci. U.S.A* **2010**, *107*, 9490−9495.

(30) Raz, Y.; Adler, J.; Vogel, A.; Scheidt, H. A.; Häupl, T.; Abel, B.; Huster, D.; Miller, Y. *Phys. Chem. Chem. Phys.* **2014**, *16*, 7710−7717.

(31) Raz, Y.; Miller, Y. *PLoS One* **2013**, *8* (8), e73303 DOI: 10.1371/journal.pone.0073303.

(32) Raz, Y.; Rubinov, B.; Matmor, M.; Rapaport, H.; Ashkenasy, G.; Miller, Y. *Chem. Commun.* **2013**, *49*, 6561−6563.

(33) Kale, L.; Skeel, M.; Bhandarkar, M.; Brunner, R.; Gursoy, A.; Krawetz, N.; Phillips, J.; Shinozaki, A.; Varadarajan, K.; Schulten, K. *J. Comput. Phys.* **1999**, *151*, 283−312.

(34) Brooks, B. R.; Bruccoleri, R. E.; Olafson, B. D.; States, D. J.; Swaminathan, S.; Karplus, M. *J. Comput. Chem.* **1983**, *4*, 187−217.

(35) MacKerell, A. D.; Bashford, D.; Bellott, M.; Dunbrack, R. L.; Evanseck, J. D.; Field, M. J.; Fischer, S.; Gao, J.; Guo, H.; Ha, S.; Joseph-McCarthy, D.; Kuchnir, L.; Kuczera, K.; Lau, F. T. K.; Mattos, C.; Michnick, S.; Ngo, T.; Nguyen, D. T.; Prodhom, B.; Reiher, W.; Roux, B.; Schlenkrich, M.; Smith, J. C.; Stote, R.; Straub, J.; Watanabe, M.; Wiorkiewicz-Kuczera, J.; Yin, D.; Karplus, M. *J. Phys. Chem. B* **1998**, *102*, 3586−3616.

(36) Jorgensen, W. L.; Chandrasekhar, J.; Madura, J. D.; Impey, R. W.; Klein, M. L. *J. Chem. Phys.* **1983**, *79*, 926−935.

(37) Mahoney, M. W.; Jorgensen, W. L. *J. Chem. Phys.* **2000**, *112*, 8910−8922.

(38) Feller, S. E.; Zhang, Y. H.; Pastor, R. W.; Brooks, B. R. *J. Chem. Phys.* **1995**, *103*, 4613−4621.

(39) Tu, K.; Tobias, D. J.; Klein, M. L. *Biophys. J.* **1995**, *69*, 2558−2562.

(40) Darden, T.; York, D.; Pedersen, L. *J. Chem. Phys.* **1993**, *98*, 10089−10092.

(41) Essmann, U.; Perera, L.; Berkowitz, M. L.; Darden, T.; Lee, H.; Pedersen, L. G. *J. Chem. Phys.* **1995**, *103*, 8577−8593.

(42) Ryckaert, J. P.; Ciccotti, G.; Berendsen, H. J. C. *J. Comput. Phys.* **1977**, *23*, 327−341.

(43) Lee, M. S.; Feig, M.; Salsbury, F. R.; Brooks, C. L. *J. Comput. Chem.* **2003**, *24*, 1348−1356.

(44) Lee, M. S.; Salsbury, J. F. R.; Brooks, C. L. *J. Chem. Phys.* **2002**, *116*, 10606−10614.

(45) Wierzejewska, M.; Wieczorek, R. *Chem. Phys.* **2003**, *287*, 169−181.

(46) Latajka, Z.; Mielke, Z.; Olbert-Majkut, A.; Wieczorek, R.; Tokhadze, K. G. *Phys. Chem. Chem. Phys.* **1999**, *1*, 2441−2448.

(47) Gumienna-Kontecka, E.; Berthon, G.; Fritsky, I. O.; Wieczorek, R.; Latajka, Z.; Kozlowski, H. *J. Chem. Soc., Dalton Trans.* **2000**, *22*, 4201−4208.

(48) Frisch, M. J.; Trucks, G. W.; Schlegel, H. B.; Scuseria, G. E.; Robb, M. A.; Cheeseman, J. R.; Scalmani, G.; Barone, V.; Mennucci, B.; Petersson, G. A.; Nakatsuji, H.; Caricato, M.; Li, X.; Hratchian, H. P.; Izmaylov, A. F.; Bloino, J.; Zheng, G. J. L. Sonnenberg, J. L.; Hada, M.; Ehara, M.; Toyota, K.; Fukuda, R.; Hasegawa, J.; Ishida, M. T.; Nakajima, T.; Honda, Y.; Kitao, O.; Nakai, H.; Vreven, T.; Montgomery, J. A.; Jr., Peralta, J.E.; Ogliaro, F.; Bearpark, M.; Heyd, J. J.; Brothers, E.; Kudin, K. N.; Staroverov, V. N.; Kobayashi, R.; Normand, J.; Raghavachari, K.; Rendell, A.; Burant, J. C.; Iyengar, S. S.; Tomasi, J.; Cossi, M.; Rega, N.; Millam, J. M.; Klene, M.; Knox, J. E.; Cross, J. B.; Bakken, V.; Adamo, C.; Jaramillo, J.; Gomperts, R.; Stratmann, R. E.; Yazyev, O.; Austin, A. J.; Cammi, R.; Pomelli, C.; Ochterski, J. W.; Martin, R. L.; Morokuma, K.; Zakrzewski, V. G.; Voth, G. A.; Salvador, P.; Dannenberg, J. J.; Dapprich, S.; Daniels, A. D.; Farkas, Ö.; Foresman, J. B.; Ortiz, J. V.; Cioslowski, J.; Fox, D. J. *Gaussian 09*; Gaussian, Inc.: Wallingford CT, 2009.

6682

dx.doi.org/10.1021/ic500387u | *Inorg. Chem.* 2014, 53, 6675−6683

(49) Zhao, Y.; Schultz, N. E.; Truhlar, D. G. *J. Chem. Theory Comput.* **2006**, *2*, 364−382.

(50) Brooks, B. R.; Bruccoleri, R. E.; Olafson, B. D.; States, D. J.; Swaminathan, S.; Karplus, M. *J. Comput. Chem.* **1983**, *4*, 187−217.

(51) Stańczak, P.; Łuczkowski, M.; Juszczyk, P.; Grzonka, Z.; Kozłowski, H. *Dalton Trans.* **2004**, *23*, 2007−2102.

(52) Valensin, D.; Luczkowski, M.; Mancini, F. M.; Legowska, A.; Gaggelli, E.; Valensin, G.; Rolka, K.; Kozłowski, H. *Dalton Trans.* **2004**, 1284−1293.

(53) Witkowska, D.; Bielinska, S.; Kamysz, W.; Kozłowski, H. *J. Inorg. Biochem.* **2011**, *105*, 208−214.

(54) Luczkowski, M.; Kozlowski, H.; Stawikowski, M.; Rolka, K.; Gaggelli, E.; Valensin, D.; Valensin, G. *J. Chem. Soc., Dalton Trans.* **2002**, 2269−2274.

(55) Matera, A.; Brasun, J.; Cebrat, M.; Swiatek-Kozłowska, J. *J. Polyhedron* **2008**, *27*, 1539−1555.

(56) Pettit, L. D.; Gregor, J. E.; Kozlowski, H. In *Perspectives in Bioinorganic Chemistry*; Hay, R. W., Dilworth, J. R., Nolan, K. B., Eds.; JAI Press: London, 1991; Vol. *1*, p 1.

(57) Kowalik-Jankowska, T.; Kozlowski, H.; Farkas, E.; Sovago, I. In *Metal Ions in Life Sciences*; Sigel, A., Sigel, H., Sigel, R. K. O., Eds.; John Wiley & Sons, Ltd., 2007; Vol. *2*, pp 63−108.

(58) Gaggelli, E.; Jankowska, E.; Kozlowski, H.; Marcinkowska, A.; Migliorini, C.; Stanczak, P.; Valensin, D.; Valensin, G. *J. Phys. Chem. B* **2008**, *112*, 15140−15150.

(59) Witkowska, D.; Valensin, D.; Rowinska-Zyrek, M.; Karafova, A.; Kamysz, W.; Kozlowski, H. *J. Inorg. Biochem.* **2012**, *107*, 73−81.

(60) Kowalik-Jankowska, T.; Ruta-Dolejsz, M.; Wiśniewska, K.; Łankiewicz, L.; Kozłowski, H. *J. Chem. Soc., Dalton Trans.* **2000**, 4511−4519.

(61) Chiera, N. M.; Rowinska-Zyrek, M.; Wieczorek, R.; Guerrini, R.; Witkowska, D.; Remelli, M.; Kozlowski, H. *Metallomics* **2013**, *5*, 214−221.

(62) Wieczorek, R.; Dannenberg, J. J. *J. Am. Chem. Soc.* **2004**, *126*, 14198−14205.

(63) http://mespeus.bch.ed.ac.uk/tanna/qg3.htm.

(64) http://mespeus.bch.ed.ac.uk/MESPEUS_10/.

(65) http://mespeus.bch.ed.ac.uk/tanna/newtargs_06.html.

(66) Liu, H.-L.; Ho, Y.; Hsu, Ch.-M. *J. Biomol. Struct. Dynam.* **2003**, *21* (1), 31−40.

(67) Lin, J.-Ch.; Ho, Y. *J. Chin. Chem. Soc.* **2005**, *52* (6), 1281−1290.